Journal of Applied Fluid Mechanics, Vol. 13, No. 3, pp. 957-967, 2020.
Available online at www.jafmonline.net, ISSN 1735-3572, EISSN 1735-3645.
DOI: 10.29252/jafm.13.03.30532

Effect of Different Flow Directions on Drag over Riblet

J. Wang[1], X. Ren[1], X. Li[1†], C. Gu[1] and M. Zhang[2]

[1] *Key Laboratory for Thermal Science and Power Engineering of Ministry of Education, Department of Energy and Power Engineering, Tsinghua University, Beijing, 100084, PR China*
[2] *Institute of Engineering Thermophysics, Chinese Academy of Sciences, Beijing 100084, PR China*

†*Corresponding Author Email: xs-li@mail.tsinghua.edu.cn*

(Received May 16, 2019; accepted November 16, 2019)

ABSTRACT

Variation in flow direction requires extensive consideration in the practical application of riblet surfaces. However, studies scarcely examine the impact of flow angle α for riblet, which is usually adopted to reduce flow drag. Accordingly, this research conducted large eddy simulation for a wide range of flow angles. We explored the effect of 0° to 90° flow angle on the surface drag change of triangular riblet. The time-averaged statistical data and instantaneous flow details indicated that skin friction is decreased with the increase in α. However, pressure drag increased much faster than the friction decrease. Result revealed that skin friction reduction by 4.537% is obtained when α=0°, and it inhibits turbulence in the spanwise direction. When α≈20°, the total drag reduction disappeared. Within this range, the deviation angle showed little influence on the total drag reduction. When α=90°, skin friction is reduced by 73.3%; however the pressure drag and total drag increased, accompanied by an increased turbulence. The flow must be nearly parallel to the riblet to achieve drag reduction. Otherwise, the transverse riblet is an effective method to increase the drag.

Keywords: Flow angle; Friction drag; Pressure drag; Triangular riblet.

NOMENCLATURE

α	flow direction
DR	skin drag reduction
D_r	shear stress on riblet wall
D_f	shear stress on smooth wall
h	the hight of riblet
H	channel height
s	the space of riblet
U	velocity component in the streamwise
V	velocity component in the normal
W	velocity component in the spanwise
X	direction in the streamwise
Y	direction in the normal
Z	direction in the spanwise
μ	dynamic viscosity
$\frac{d\overline{U}}{dy}$	velocity gradient
$(\,)^+$	normalization in law of the wall variables
$\overline{(\,)}$	average of ( ) in time and in the homogeneous spatial directions
$(\,)_{rms}$	root-mean-square value of ( )

1. INTRODUCTION

In recent years, scholars have extensively studied riblet as a type of passive drag reduction device Walsh (1978) from the NASA Langley Research Center investigated the influences of different shapes, sizes, and flow speeds on the drag reduction effect of the riblet from the early stage and found that the V-shaped riblet can reduce drag by 8% (Walsh *et al*. (1982; 1983; 1984). Other scholars have conducted studies on the riblet distributed along the flow direction. Clark (1990) and Tang and Clark (1993) conducted flow visualization experiments on a near-wall turbulent boundary layer with the riblet arranged along the flow direction to explore turbulence activities and flow field characteristics. They proposed the concept of "riblet sublayer" and asserted that one of the main functions of riblet is to prevent high-speed fluid from flowing into the near wall. Stalio and Nobile (2003) used the direct numerical simulation (DNS) method to study the triangular riblet distributed along the flow direction. Such task aimed at analyzing flow and heat transfer in laminar and

turbulent regimes. The aforementioned authors noted that the heat transfer efficiency of the riblet surface is lower than that of the flat plate in the laminar flow. Such case is also observed in turbulent flow and is inconsistent with previous experiments. In the case of drag reduction and increase, Ng *et al.*(2014) used the DNS calculation method to analyze the effect of riblet size on the flow field and evaluate the correlation between riblet size and the resultant flow field by using the newly proposed parameter. Experimental and numerical simulation studies on drag reduction and riblets have focused on the flow direction arrangement of the riblet. Several other studies have focused on the transverse riblet. Ikeda and Durbin (2007) used the DNS method to study a rectangular riblet perpendicular to the flow direction of a low wall in channel, derived instantaneous flow field and turbulence statistics. They found different turbulent structures on the two walls, with long stripes on the smooth wall and irregular vortices on the riblet wall. Leonardi *et al*. (2004) studied the transverse rectangular rib with different ratios of riblet height to riblet spacing with DNS. The result showed that the streamwise length of a turbulent structure near the wall of a riblet can be decreased and the spanwise length can be increased relative to that of a smooth surface.

Many successful applications have been explored for the drag reduction effect of the riblet. For example, in the aerospace field, Mclean *et al*. (1987) from the NASA Langley Research Center applied symmetrical V-shaped riblet vinyl films of the 3M Company to the upper wing of the T-33 aircraft and measured the drag reduction rate up to 6%. German DLR-coated riblets were applied to 70% of the area of the A320 aircraft, with a drag reduction set to 3% in a flight test (Bechert *et al*. 2000). Viscous resistance in the turbulent boundary layer is the major factor in the rise of airline fuel costs (Flandoli *et al*. 2010). Coustols and Cousteix (1990) used the 3M riblet on the upper surface of the LC100D wing to test and measure drag, in which the flow angle was set from 0° to 6°. At 0° and 2°, a 2% total drag reduction, which corresponded to 7% viscous drag reduction, was obtained without drag reduction effects observed at the high angles. This finding can be partly explained by the effect of boundary layer separation. Walsh (1982) applied the symmetrical triangular riblet to a conventional aircraft and experimentally investigated the drag reduction effect of the riblet with a deflection of 0° and 15° in the same h^+ (dimensionless height) range. The results showed that friction drag reduction was almost unaffected by the 15° deflection.

In practical applications, the riblet film is manufactured and applied to a certain surface in a fixed single pattern. However, the flow direction on the riblet surface in the actual flow field is unnecessarily positioned along the placement direction of the riblet or in a certain fixed direction, such as the vertical riblet direction. Studies on the effect of incidence angle on riblet drag reduction are rare, and the incidence angle range is small. No research seems to have been conducted on the angle α formed between the riblet and the incoming flow under the wide-range variation condition. Thus, this research focuses on the angle under the wide-range variation condition. The rib arrangement is fixed, and α is changed to control the flow direction. The large eddy simulation (LES) method is used to investigate the effects of different α (angle of deviation from riblet, representing the flow direction) on the drag reduction of the riblet wall and the influence of the flow field in the range of 0—90°.

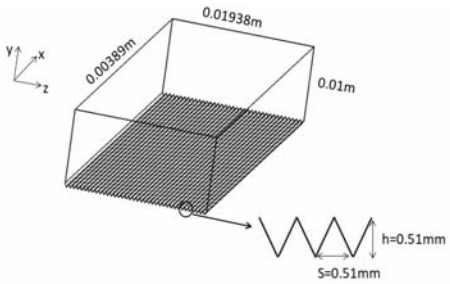

Fig. 1. Computational domain and geometric size.

2. NUMERICAL METHODS

The LES method is employed to numerically simulate the riblets (h=s=0.51 mm, where h and s represent the height and spacing of the riblets [symmetrical triangular or V-shaped], respectively). The riblet has an optimal drag reduction effect in the Walsh's test. The change in the flow direction angle is explored to determine the influences of flow angle on wall shear stress, pressure resistance, drag reduction and flow field (or corresponding flow characteristics) in this study. The calculation domain is the channel with different upper and lower walls. Straight triangular riblets are distributed along the x direction of the lower wall in the Cartesian coordinate system, and the upper wall is a smooth plate. Here, the velocity components of each point in the x, y, and z directions are u, v, and w respectively. The streamwise, normal and spanwise directions are denoted by X, Y and Z respectively. The velocities in the three directions are denoted by U, V, and W. Figures 1 and 2 show the computational domain and grid situation near the wall. The mesh is divided by a hexahedral grid, refined in the wall vicinity in the y direction, and uniformly distributed in the x and z directions. Table 1 lists the three different distribution sets in the three directions and corresponding mesh parameter for α=0°. On the basis of the number of grid, scheme 2 with a moderate amount of grid is finally selected as the mesh used for computation in all cases. The corresponding step sizes in each direction are given in wall units. A Y-block division is adopted in a triangular groove. Figure 3 shows the mesh distribution inside the groove. The minimum and maximum mesh spacing values in the wall units in the y direction are computed as

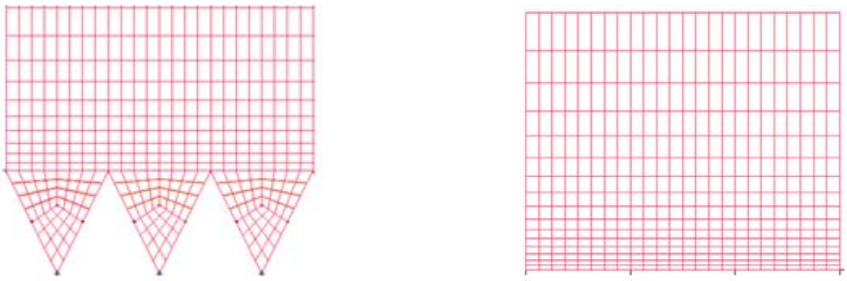

(a) Riblet Wall (b) Smooth Wall

Fig. 2. Details of the mesh near the wall.

Table 1 Mesh parameters

Scheme	N=Nx×Ny×Nz	Δx^+	$\Delta y^+_{\min}$	$\Delta y^+_{\max}$	Δz^+
1	106×60×342	14.78	0.88	14.36	2.54
2	128×73×342	12.21	0.88	8.10	2.54
3	154×85×342	10.14	0.88	6.09	2.54

$\Delta y^+_{\min} = 1.55$, $\Delta y^+_{\max} = 1.75$ and $\Delta y^+_{\min} = 0.88$, $\Delta y^+_{\max} = 8.10$ inside and outside the groove, respectively. The calculations in this research have adopted the same set of calculation domain and grid, and only α and mass flow rate are changed to ensure consistency in velocity in the flow direction. The incoming velocity is approximately 10 m/s. The α range is 0° to 90°. α=0° and 90° are the mainstreams for x and z, respectively. The other angles are between the x and the z directions.

The Reynolds number based on $H/2$ (i.e., half of the channel height) and mainstream velocity is approximately 3,550 in the calculations. The upper and lower boundaries correspond to the wall without slip. The inlet and outlet and the sides are in periodic boundary conditions. The inlet and outlet correspond to the given mass flow rate and flow direction. The laminar results are taken as the initial field for calculation. The LES unsteady calculation is carried out, and the WALE model is selected. The time-step is set to be 2e-5 s. Once the calculation has reached a stable state of turbulence, the statistical quantities are averaged over time.

3. Analysis And Discussion

3.1 Drag Variations on Walls

Here, the calculation for α=0° is consistent with the conditions provided by a previous study (Walsh 1982). Computational reliability is verified by comparing the drag reduction results. The time averaged skin friction reduction calculated in this research is -4.537%, which corresponds to a h^+ of 20.34. When h^+≈20, the corresponding drag reduction is approximately -4% in Walsh's experiment. The results calculated in this work are within the range of drag reduction in Bechert *et al.*'s (1997) experiment. The skin friction drag reduction is -73.3%, and the corresponding h^+ is 21.41 for α=90°. The skin friction drag reduction can be calculated as follows:

$$DR = \frac{D_r - D_f}{D_f} \times 100\% \ , \tag{1}$$

here D_r and D_f represent the drag of the riblet and smooth surfaces, respectively.

The forces presented in this work are the results of time averaging. Figures 3 and 4 show the component and total forces of the smooth and riblet walls with the increase in α. Viscous resistance consists of two parts, namely, pressure drag and skin friction. When α is changed, the surface pressure of the riblet structure also significantly changes.

Figure 3(a) shows that the frictional drag component in the x direction rapidly decreases when α increases on a smooth plate. However, the z component slowly increases with the increase in α. When the angle between the flow direction and a certain coordinate direction is small, the force component along this coordinate direction dominates. The force change in this direction is slow when the angle is small. The total drag on the upper plate remains essentially the same. The riblet surface has a uniform V-shaped structure. The z skin friction increases in the reverse direction with the increase in α, indicating a linear relationship with α. The pressure drag component in the z direction linearly increases with the increase in α. The increase in speed is much faster than the decrease in skin friction toward the z direction. The force in the x direction slightly changes when the angle changes within 20° with the flow angle increase. When the flow angle is greater than 20°, the friction resistance in the x direction linearly decreases with the incoming flow angle. This phenomenon can be explained as follows: within a

certain small angle range, the α increase leads to the decrease in streamwise velocity, the increase in turbulence intensity, and the constant skin fraction within a certain range. Accordingly, the total drag on the riblet surface rapidly increases with the increase in α. In α=90°, pressure drag is the main viscous drag of the rough wall, and it accounts for 117% of the total resistance. This value is similar to that reported by Ikeda and Durbin (2007). Figure 4 demonstrates that the riblet exhibits a drag reduction effect when the angle is less than 20°. When the inlet flow angle continues to increase to approximately 20°, the riblet surface force significantly changes. Within the drag reduction range, the deviation angle has little influence on drag reduction. Walsh (1982) verified that the 15° deviation has little effect on the drag reduction

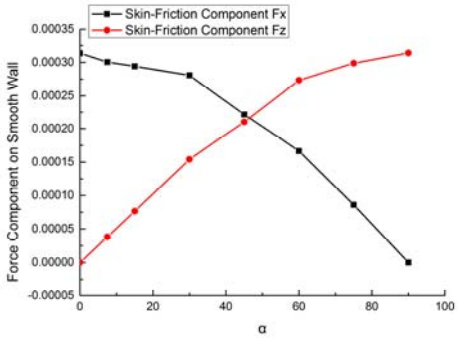

(a) Component of force on a smooth wall

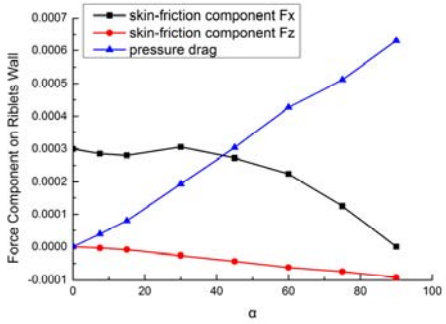

(b) Component of force on a riblet wall

Fig. 3. Component of force on smooth and riblet walls with α variations.

of a triangular riblet. By contrast, the 30° deviation has no drag reduction effect. This finding is consistent with the study results. Skin friction largely decreases with the increase in α. However, pressure resistance also increases accordingly, resulting in a slowly disappearing drag reduction. The same flow direction with the riblet is assumed to effectively reduce the drag. Otherwise, the opposite effect will be observed.

3.2 Detailed analysis of Average flow Field at α=0° and α=90°

This research mainly analyzes the two special cases (i.e., α=0° and α=90°) of statistical data. The analyses below begin with the discussion on the time-averaged data, which were obtained by collecting the 5,000 time-step data for time-averaged processing after calculation convergence.

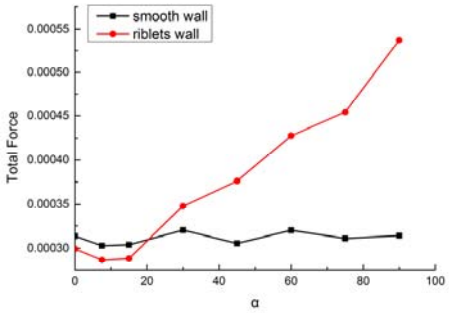

Fig. 4. Total force on the smooth and riblet walls with α variations.

3.2.1 Time-Averaged Velocity Distribution

Figure 5 shows the distribution of the time-averaged streamwise velocity along the normal direction of the two groups of examples and their partial magnification. Figure 6 shows the instantaneous velocity vector distribution inside the groove in the two cases. In Fig. 5, the velocity increases slowly inside the riblet and dramatically increases above the riblet tip, when α=0°. The velocity gradient maintains a high value within a certain normal height. This value is bigger than that when α=90°. According to the shear stress formula,

$$\tau_w = \mu \frac{d\overline{U}}{dy}, \tag{2}$$

where τ_w is the shear stress on the wall, μ is the dynamic viscosity, and $\frac{d\overline{U}}{dy}$ is the velocity gradient near the wall. The shear stress is large when $\frac{d\overline{U}}{dy}$ is high. This relationship suggests that the skin friction of the riblet is high at α=0°. The velocity gradient is much smaller near the riblet than that in the upper plate. The skin friction of the riblet is reduced in both cases, however, when α=90°, such friction is reduced futher. The definition of the boundary layer thickness indicates that if speed is consistent with the mainstream speed of 99%, then, the corresponding *y*/*H* values are 0.41 and 0.54 at at α=0° and 90°, respectively. Therefore, vertical inflow is assumed to increase the boundary layer thickness.

The difference between the above-mentioned two cases can be explained by the α effect of on the flow field. Figure 6 is the velocity vector diagram of the resultant velocity. Figures 5 and 6 demonstrate that the speed values in the groove in the two cases have extremely low values. The fluid in the groove is restricted, and no movement can be seen perpendicular to the flow direction when α=0°. The fluid in the groove tends to be calm, and it is in

a quiet laminar flow state. The larger vortex is restricted outside the groove because of the riblet structure, and it cannot directly cause friction on the surface. Many scholars believe that the drag of riblet arranged in the flow direction can be reduced because the riblet itself inhibits the development of vortices in a spanwise direction (Bechert *et al.* 1986; Bechert and Bartenwerfer 1989; Goldstein *et al.* 1995; Choi 1989). When α=90°, the velocity value in the groove is extremely low due to the viscosity and the riblet geometric configuration, while the fluid within the groove is in an active motion state. A pressure difference is formed in front and behind the groove, and a secondary flow (vortex zone) is generated in the groove as the fluid flows through the surface. A backflow opposite to the main flow direction is formed inside the grooves. The velocity is negative, further resulting in a negative friction drag in the groove. At the place where the top of the groove is close to the main flow, the vortices moving within the groove and the action of the main flow will weaken the velocity value of the contact layer. Consequently, the velocity near the riblet wall and friction is reduced. When the angle between the incoming flow direction and the riblet is large, vortices can be generated on the riblet surface to enhance turbulence. The friction on the riblet surface is reduced due to the vortices in the groove opposite the flow direction. However, the increase in pressure resistance becomes dramatic. Accordingly, viscous drag continuously increases.

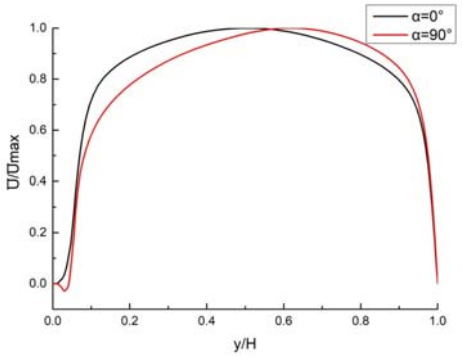

(a) Overall velocity distribution

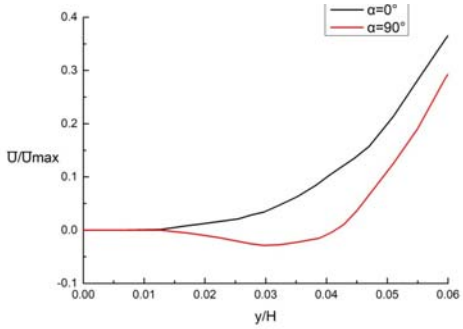

(b) Internal velocity distribution of the riblet

Fig. 5. Velocity distribution in the normal direction.

3.2.2 Velocity Profile

Figure 7 shows the velocity profiles at α=0° and 90°. The method proposed by Hooshmand *et al.* (1983) is employed to obtain the virtual origin on the riblet surface in the figure. A *y*-*U* curve fitting is conducted on the linear area of velocity distribution near the riblet top, in which the intercept of the fitting line corresponds to the position of the virtual origin on the riblet surface. The velocity profile of the smooth surface in the figure is consistent with the empirical theory for the viscous sublayer and logarithmic law region. The velocity profile of the logarithmic law region of the riblet at α=0° slightly moves up and the intercept increases from 5.5 to 6.2 compared with the logarithmic law region of the smooth surface. Lumley (1973) reported that the upward movements in the logarithmic law is closely related to the balance between turbulent energy generation and viscous dissipation. An upward shift of the logarithmic law corresponds to the reduction of skin friction drag. Aupoix *et al.* (2012), Hooshmand *et al.* (1983), and Okabayashi *et al.* (2014) also agree with this view. With regard to the curve of the α=90° riblet, the logarithmic law region also moves up, but the slope and intercept change. The combined analysis in Figures 4 and 5 indicate that, in the α=90° condition, the skin friction drag reduction is high, and the logarithm law shifts upward even further when such friction on the riblet surface is small.

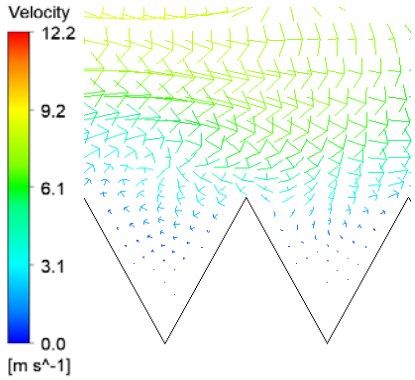

(a) α=0°

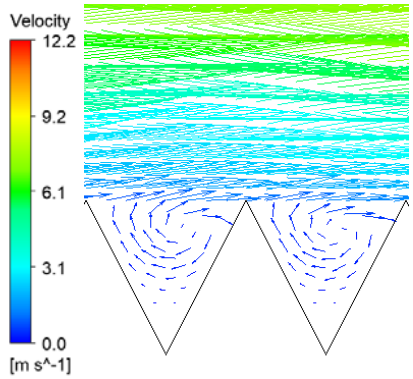

(b) α=90°

Fig. 6. Resultant velocity vector distribution inside the groove.

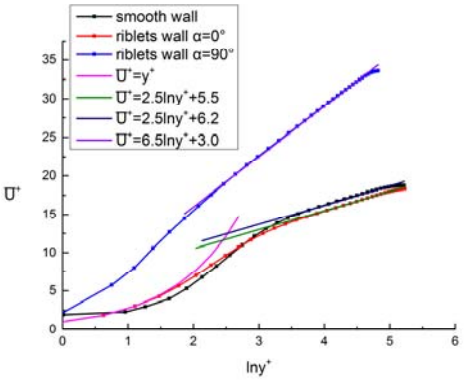

Fig. 7. Velocity profile.

3.2.3 Distribution of Root- Mean- Square (RMS) Values of Fluctuation Velocity

Figure 8 shows the RMS values of fluctuation velocity in three directions. The ordinates are dimensionless with the maximum time-averaged streamwise velocity in each condition. First, the RMS values of fluctuation velocity near the riblet are less than those near the smooth wall in three directions when α=0°. In the DNS study conducted by Choi *et al.*(1993), the three components of turbulence intensity can be reduced in the drag reduction structure of the longitudinal triangular riblet. The normal and spanwise velocity fluctuations can be reduced by 10%. By contrast, the streamwise velocity fluctuation can be reduced by 5%. In this study, the peak value of pulse velocity in the three directions on the side of the riblet decreased and stayed away from the wall. This notion indicates that the riblet can reduce the turbulence near the wall. Similar findings have been verified by Chu and Karniadakis (1993). The findings for the mainstream region of the RMS fluctuation velocity curves in the three directions are consistent with those for the smooth surface, in which the drag reduction effect of the α=0° riblet is manifested near the wall. This finding is also consistent with that of Setkauskas and Vysniauskiene (2002). The RMS value of fluctuation velocity near the groove becomes slightly weaker than that near the smooth surface when α=90°. The maximum value is almost the same as that on the smooth plate in the streamwise case, and it is substantially greater than those for the smooth plate in the other two directions. The α=90° fluctuation velocity value is increased until it reaches the mainstream region in all three directions. This case indicates that the riblet can entirely strengthen the flow pulsation.

The common feature of the near-riblet case when α=0° and 90° is represented by the curve near the riblet shifting to the right of the plate, which is caused by the groove on the riblet surface. The velocity pulsation decreases in the groove (y/[0.5H]≈0.1). The fluid with high turbulence is pushed away from the surface due to the continuous fluid flow, thereby resulting in the thickened boundary layer near the riblet wall. However, the movement to the right for α=0° is more apparent than that for α=90°. The manifestation suggests that turbulence can develop close to the riblet wall when α=90°. In summary, the riblet can easily induce turbulence generation and increase turbulence strength when α=90°.

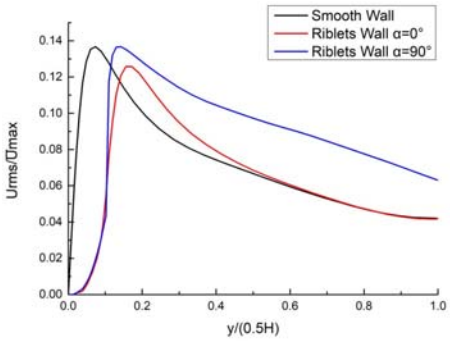

(a) RMS fluctuation velocity in the streamwise direction

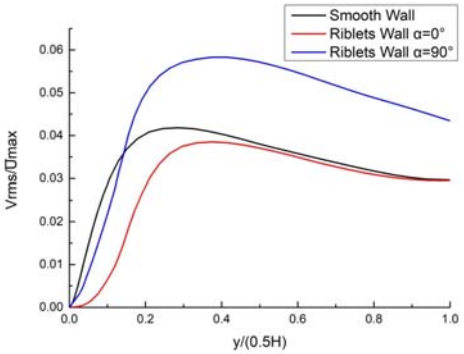

(b) RMS fluctuation velocity in the normal direction

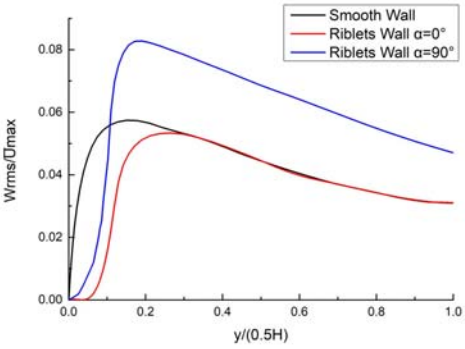

(c) RMS fluctuation velocity in the spanwise direction

Fig. 8. RMS fluctuation velocity.

3.2.4 Reynolds stress distribution

Figure 9 shows the turbulent shear stress distribution. The momentum exchange caused by turbulence pulsation becomes more apparent on the smooth surface than that on the riblet surface when α=0°. The Reynolds stress decreases near the wall, but it is consistent on the upper plate in the region far from the wall. The drag reduction was tested

near the riblet wall but not in the main flow region to verify α=0°,. Suzuki and Kasagi (1994) found that the velocity fluctuation and the Reynolds stress near the riblet wall were lower than those on the flat plate in their triangular riblet wall experiment with the drag reduction effect in the longitudinal arrangement even if the flow fields were similar between the riblet and smooth walls. However, the Reynolds stress is in the local extremum near the riblet when α=90° because vortices are generated in the reverse flow direction in grooves. Despite the slow movement of fluid in the groove, it has a certain degree of turbulence. In the main flow region, velocity pulsation has notably strengthened, thus enhancing turbulence intensity, momentum exchange, and mass transfer and dissipation. Figures 3 and 4 demonstrate that skin friction decrease is relatively high when α=90°, but turbulence intensity substantially increases. At this time, any beneficial effect is overwhelmed by the harmful effect of the enhanced turbulent shear stress.

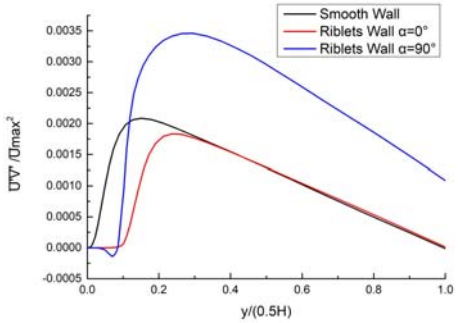

Fig. 9. Reynolds stress distribution.

3.3 Instantaneous flow Field at α=0° and 90°

The flow fields at the instantaneous moment are determined when the viscous drag reduction has the time-averaged values at α=0° and α=90°.

3.3.1 Wall Shear Stress Contours

Figure 10 shows the resultant wall shear stress contours on the smooth and riblet walls at α=0° and 90° in an instantaneous moment, particularly when the drag reduction is close to the time-averaged drag reduction. The high and low values of shear force in the upper wall are distributed alternatively and in a strip pattern in the flow direction. The overall value of the wall shear stress on the smooth wall is consistent at α=0° and 90°. The distribution curve of the time-averaged skin friction manifests that the values of the time-averaged wall shear stress on the smooth wall are all in the order of 3e-4. By contrast, the α=90° riblet generally has a smaller wall shear stress value, which corresponds to the deeper blue area in the figure, than that of α=0°. This finding suggests higher skin friction reduction. The shear stress value distributed. near the top of the groove is large, when α=0°, whereas most other regions have small shear stress values. This phenomenon conforms with the conclusion that the bottom of the riblet has a significant drag reduction effect, whereas the top part has none. The significant drag reduction effect of the bottom part can compensate the large wet area. The shear stress distribution on the riblet surface still has a longitudinal strip pattern due to the riblet existence. The wall shear stress distribution over the riblet is relatively uniform when α=90°. Extremely high value regions become non-existent, and the strip structure in the vertical flow direction becomes non-apparent.

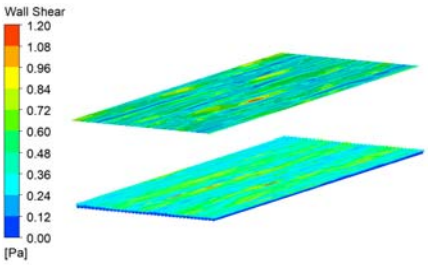

(a) α=0°

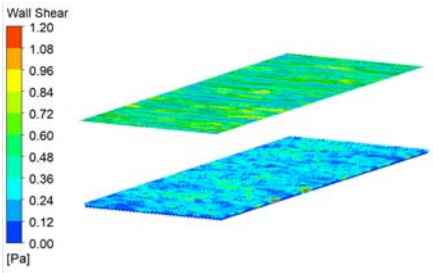

(b) α=90°

Fig. 10. Resultant wall shear stress contours.

3.3.2 Pressure Contours on the Wall

Figure 11 shows the pressure distribution on the smooth and riblet walls. The upper and lower walls at α=0° have pressure spots with prominently high and low values, respectively. The lower wall pressure spots at α=90° have evident distribution, whereas the upper ones have no obvious distribution. These findings indicate that the upper wall pressure at α=90° has a smaller change range than the lower wall pressure. The upper and lower wall pressure changes are consistent at α=0°. The comparison between the two images shows that the pressure range corresponding to α=90° is relatively large. The large and smalle pressures are distributed on the riblet wall. The figure further indicates that setting the angle to α=90° changes the pressure distribution on the wall. Accordingly, the pressure range of the riblet wall increases and the pressure differential resistance is remarkably enhanced.

3.3.3 Velocity Strip at y^+=20

Figure 12 shows the resultant velocity contours at y^+=20. The two figure insets, demonstrate that high and low velocity bands are distributed around the upper and lower walls in the flow direction. The comparison result of the upper and lower surfaces when α=0°, reveals that the upper surface appears

with a wide high-speed band. By constrast, the low surface has many small low-speed bands in the entire flow direction of the calculation domain. In general, the velocity value of the lower side is lower than that of the upper side. The high and low speed bands on the upper side are densely interlaced, and the high speed ones appear in most parts of the region when α=90°, However, the speed band consistency at α=90° is poorer than that at α=0° near the riblet side. The speed strip at y^+=20 in the streamwise direction is intermittent when α=90°. The vortex band in the streamwise direction is affected by the groove. The reverse vortex generated in the groove has a certain influence on the flow within a certain normal distance above the riblet, which inhibits the occurrence of the streamwise vortex in the flow direction.

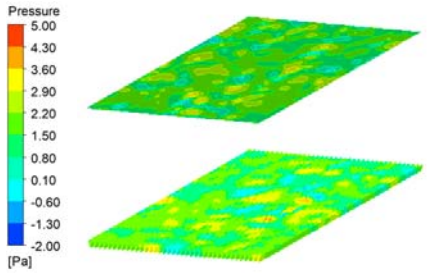

(a) α=0°

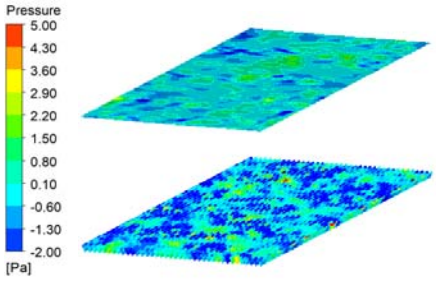

(b) α=90°

Fig. 11. Pressure contours on the walls.

3.3.4 Vorticity Contours

Figure 13 shows the vorticity distribution at x=0.02 m and z=0.000255 m. Figure 13(a) shows the vorticity distribution on the cross section perpendicular to the flow at α=0° and α=90°. The vorticity continuity in the spanwise direction and the upward sweep in the normal direction will lead to the shedding and breaking of the vortices. Figure 13(b) shows the vorticity distribution on the section along the direction of the incoming flow. The vorticity distribution stability in the streamwise direction indicates that the corresponding vortices have moderately changed when α=0°. The sweeping movement of the flow in the streamwise direction coincides with the vortex development process when α=90°. Moreover, the vortex tends to roll up and move out of the flow layer. This separation movement enhances the breaking of the vortex and increases turbulence.

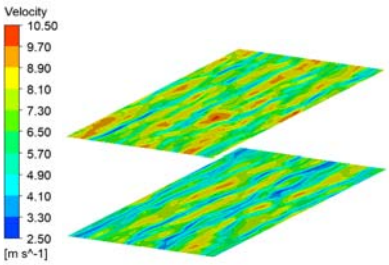

(a) α=0°

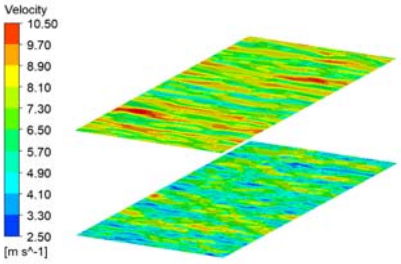

(b) α=90°

Fig. 12. Resultant velocity contours at y^+=20.

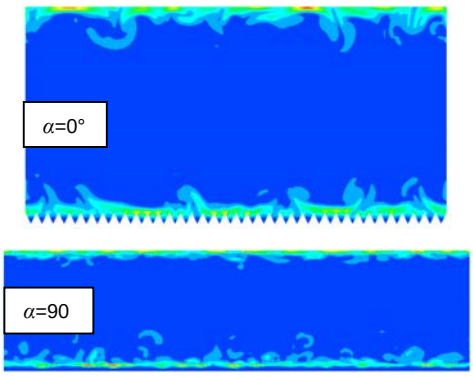

(a) Cross section perpendicular to the flow direction

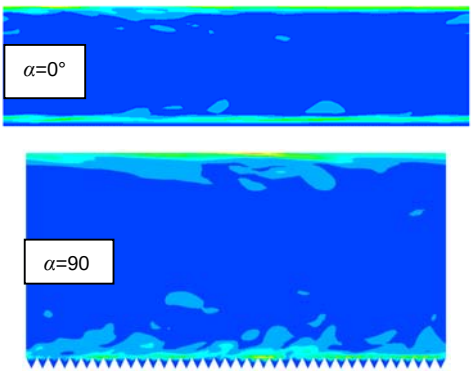

(b) Cross section in the flow direction

Fig. 13. Vorticity contours.

3.3.5 Streamline Distribution

Figure 14 shows the resultant velocity streamline at

x=0.02 m and z=0.000255 m section at α=0° and α=90°. A certain amount of fluid with low velocity runs through the groove when α=0°, in which the cross section is perpendicular to the flow at x=0.02 m. Fluid velocity begins to sharply increase near the groove top, and multiple pairs of counter rotating vortices appear above the riblet surface. However, the development of vortices perpendicular to the flow direction is difficult to observe in the longitudinal section (z=0.000255 m). When α=90°, particularly in the x=0.02 m section, lateral fluid flows through the riblet surface, and low-speed fluid occupies the interior of the grooves and entirely swirls within them. The skin friction on the surface of the riblet at α=90° is lower than that at α=0°, and its skin friction reduction is greater. A vortex is formed in the grooves, and the velocity value is negative. Specifically, the velocity is opposite to the incoming flow direction, which is consistent with the distribution of the time-averaged velocity with normal distance (Fig. 5). The low velocity fluid near the wall can help avoid high-energy exchange and loss and reduce wall drag.

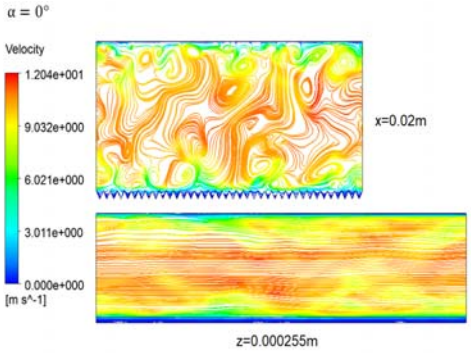

(a) Transverse section

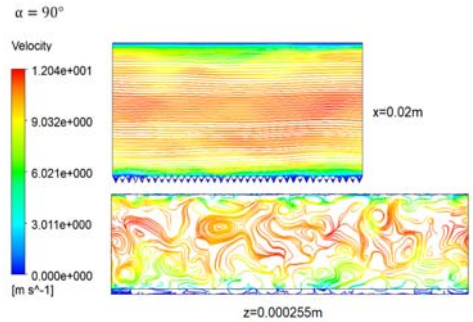

(b) Longitudinal section

Fig. 14. Resultant velocity streamlines.

3.3.6 Vortex Distribution

Figure 15 shows the vortex at α=0° and 90°; then , it is calculated and colored by using the Q criterion at Q=0.06. The difference between the upper and lower walls of the two cases shows α=90°, in which the vortex on the riblet wall is dense, and the turbulence activities are strong. The turbulence intensity dramatically increased than that of the smooth wall. The comparison result of α=0° and α=90° reveals that the overall case at α=0° of the overall vortex is small, and the distribution of streamwise vortices on the lower wall is concentrated. This finding can be explained by the incoming flow in the same direction as that in the riblet structure. Most fluids near the wall attach to the surface for movement. By contrast, the riblet's unique groove structure limits the streamwise vortex to the outside of the groove. Flow develops on the top of the rib, further showing a streamwise vortex band. In summary, the vortex on the lower wall is less than that on the upper wall. Specifically, the riblet structure inhibits the vortex development. The figure also shows that the spanwise development of the vortex is inhibited. The vortex density difference between the upper and lower walls is huge when α=90°. The streamwise vortex distribution on the upper wall is uniform. The vortex density on the lower wall is increased, the vortex on the wall is relatively small, and the vortex on the outer region from the wall is increased. Near the riblet wall, a complete layer of fine vortices covers the top of the riblet, indicating uniform turbulence characteristics. The vortex zone is broken into a small vortex that occupies a wide region above the riblet wall, thus enhancing turbulence above the riblet wall.

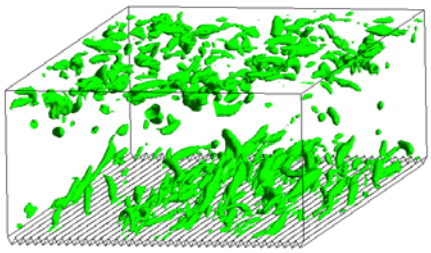

(a) α=0°

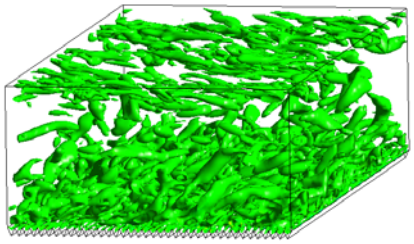

(b) α=90°

Fig. 15. Vortex distribution.

4. CONCLUSIONS

This study employed the LES method to determine the drag reduction effect of different flow directions on the longitudinal arrangement of the V-shaped riblet. It also explored the mechanism of the riblet action on the flow field by comparing it with the smooth plate. The research findings are summarized as follows:

(1) The total drag on the riblet surface is 4.537%

less than that in the smooth surface when α=0°. When α is smaller than 20°, the total drag on the riblet surface has little change and still has a drag reduction effect. The total drag on the riblet surface was approximately 1.7-fold as large as large as that of the smooth surface when α=90°.

(2) The skin friction on the riblet surface decreases whereas the pressure drag increases with the increase in inlet flow angle. The pressure drag increases faster than the decreasing skin friction.

(3) The action mechanisms of the riblet in the longitudinal flow and the transverse flow differ. In the longitudinal flow, the riblet structure limits the spanwise development of turbulence. Accordingly, turbulence weakens, and skin friction reduces. In the transverse flow, the riblet structure enhances turbulence. The transverse vortices generated within the riblet reduce the skin friction to zero, or even to negative values. However, the pressure resistance generated is much greater than the reduced skin friction, thus increasing the total drag.

Thus, the flow direction should be parallel to the riblet when the riblet is used for drag reduction. The transverse riblet is an effective method if the goal is to increase drag.

ACKNOWLEDGEMENTS

This study is supported by the Projects 51736008 of the National Natural Science Foundation of China and 2017-II-0007-0021 of the National Science and Technology Major Project of China.

REFERENCES

Aupoix B. , Pailhas G. and Houdeville, R. (2012) . Towards a general strategy to model riblet effects, *AIAA Journal* 50 (3), 708-716.

Bechert, D. W., Bruse, M., Hage, W. and Meyer, R. (2000). Fluid mechanics of biological surfaces and their technological application, *Naturwissenschaften* 87 (4), 157-171.

Bechert, D. W., & Bartenwerfer, M. (1989). The viscous flow on surfaces with longitudinal ribs, *Journal of Fluid Mechanics* 206(-1), 105.

Bechert, D. W., Bruse, M., Hage, W., Vander Hoeven, J. G. T. and Hoppe, G. (1997). Experiments on drag-reducing surfaces and their optimization with an adjustable geometry, *Journal of Fluid Mechanics* 338, 59-87.

Bechert, D. W., Bertenwerfer, M., Hoppe, G. and Reif W.-E. (1986). Drag reduction mechanisms derived from shark skin, *American Institute of Aeronautics and Astronautics* 2, 1044.

Choi, H., Moin, P. and Kim, J. (1993). Direct numerical simulation of turbulent flow over riblets, *Journal of Fluid Mechanics* 255(-1), 503.

Choi, K. –S. (1989). Near-wall structure of a turbulent boundary layer with riblets, *Journal of Fluid Mechanics* 208 (-1), 417.

Chu, D. C. and Karniadakis, G. E. (1993). A direct numerical simulation of laminar and turbulent flow over riblet-mounted surfaces, *Journal of Fluid Mechanics* 250 (-1), 1.

Clark, D. G. (1990). Boundary layer flow visualisation patterns on a riblet surface, *Turbulence Control by Passive Means* 4, 79-96.

Coustols, E. and Cousteix, J. (1990). Experimental investigation of turbulent boundary layers manipulated with internal devices: riblets, IUTAM Symp, *Structure of Turbulence and Drag Reduction* 557-584.

Flandoli, F., Berselli, L. C., Kyed, M. and Bemelmans, J. (2010). Advances in mathematical fluid mechanics, *Incompressible Bipolar and Non-Newtonian Viscous Fluid Flow* 271-284.

Goldstein, D., Handler, R. and Sirovich, L. (1995). Direct numerical simulation of turbulent flow over a modeled riblet covered surface, *Journal of Fluid Mechanics* 302 (302), 333-376.

Hooshmand, D., Youngs, R. and Wallace, J. M. (1983). An experimental study of changes in the structure of a turbulent boundary layer due to surface geometry changes, *AIAA Paper*, 230.

Ikeda, T. and Durbin P. A. (2007). Direct simulations of a rough-wall channel flow, *Journal of Fluid Mechanics* 571, 235-263.

Leonardi, S., Orlandi, P., Djenidi, L. and Antonia, R. A. (2004). Structure of turbulent channel flow with square bars on one wall, *International Journal of Heat and Fluid Flow* 25 (3), 384-392.

Lumley, J. L. (1973). Drag reduction in turbulent flow by polymer additives, *Journal of Polymer Science Part A Polymer Chemistry* 7 (1) -

Mclean, J. D., George-Falvy, D. N. and Sullivan, P. P. (1987). Flight-test of turbulent skin-friction reduction by riblets, In *Proceedings of the International Conference*, London, England, United Kingdom, 15-17, 408-24.

Ng, J. H., Jaiman, R. K. and Lim, T. T. (2014). Direct numerical simulation of geometric effects on turbulent flows over riblets, *7th AIAA Flow Control Conference*, June 2014, Atlanta, GA

Okabayashi, K., Matsue, T., Asai, M. and Naito, H. (2014). Rans modeling for flows on riblets based on experimental data, *29th Congress of the International Council of the Aeronautical Sciences*, September 2014, St. Petersburg, Russia.

Setkauskas, V. and Vysniauskiene, Z. (2002).

Investigation of ribbed plate vibrations in viscous fluid, *Mechanika* 3 (35), 34-37.

Stalio, E. and Nobile, E. (2003). Direct numerical simulation of heat transfer over riblets, *International Journal of Heat and Fluid Flow* 24 (3), 356-371.

Suzuki, Y. and Kasagi, N. (1994). Turbulent drag reduction mechanism above a riblet surface, *AIAA Journal* 32 (9), 1781-1790

Tang, Y. P. and Clark, D. G. (1993). On near-wall turbulence-generating events in a turbulent boundary layer on a riblet surface, *Applied Scientific Research* 50 (3-4), 215-232.

Walsh, M. J. (1982). Turbulent boundary layer drag reduction using riblets, *20th Aerospace Sciences Meeting*, January 1982, Orlando, FL, U.S.A.

Walsh, M. J. (1983). Riblets as a viscous drag reduction technique, *AIAA Journal* 21 (4), 485-486.

Walsh, M. J. and Lindemann, A. M. (1984). Optimization and application of riblets for turbulent drag reduction, *22nd Aerospace Sciences Meeting*, January 1984, Reno, NV, U.S.A.

Walsh, M. J. and Weinstein, L. M. (1978). Drag and heat transfer on surfaces with small longitudinal fins, *11th Fluid and Plasma Dynamics Conference*, July 1978, Seattle, WA, U.S.A.